Fermilab-PUB-97/093-E
April 16, 1997

Properties of Six-jet Events with Large Six-jet Mass at the Fermilab Proton-Antiproton Collider

F. Abe,[17] H. Akimoto,[36] A. Akopian,[31] M. G. Albrow,[7] S. R. Amendolia,[27] D. Amidei,[20] J. Antos,[33] S. Aota,[36] G. Apollinari,[31] T. Asakawa,[36] W. Ashmanskas,[18] M. Atac,[7] F. Azfar,[26] P. Azzi-Bacchetta,[25] N. Bacchetta,[25] W. Badgett,[20] S. Bagdasarov,[31] M. W. Bailey,[22] J. Bao,[39] P. de Barbaro,[30] A. Barbaro-Galtieri,[18] V. E. Barnes,[29] B. A. Barnett,[15] M. Barone,[9] E. Barzi,[9] G. Bauer,[19] T. Baumann,[11] F. Bedeschi,[27] S. Behrends,[3] S. Belforte,[27] G. Bellettini,[27] J. Bellinger,[38] D. Benjamin,[35] J. Benlloch,[19] J. Bensinger,[3] D. Benton,[26] A. Beretvas,[7] J. P. Berge,[7] J. Berryhill,[5] S. Bertolucci,[9] B. Bevensee,[26] A. Bhatti,[31] K. Biery,[7] M. Binkley,[7] D. Bisello,[25] R. E. Blair,[1] C. Blocker,[3] A. Bodek,[30] W. Bokhari,[19] V. Bolognesi,[2] G. Bolla,[29] D. Bortoletto,[29] J. Boudreau,[28] L. Breccia,[2] C. Bromberg,[21] N. Bruner,[22] E. Buckley-Geer,[7] H. S. Budd,[30] K. Burkett,[20] G. Busetto,[25] A. Byon-Wagner,[7] K. L. Byrum,[1] J. Cammerata,[15] C. Campagnari,[7] M. Campbell,[20] A. Caner,[27] W. Carithers,[18] D. Carlsmith,[38] A. Castro,[25] D. Cauz,[27] Y. Cen,[30] F. Cervelli,[27] P. S. Chang,[33] P. T. Chang,[33] H. Y. Chao,[33] J. Chapman,[20] M. -T. Cheng,[33] G. Chiarelli,[27] T. Chikamatsu,[36] C. N. Chiou,[33] L. Christofek,[13] S. Cihangir,[7] A. G. Clark,[10] M. Cobal,[27] E. Cocca,[27] M. Contreras,[5] J. Conway,[32] J. Cooper,[7] M. Cordelli,[9] C. Couyoumtzelis,[10] D. Crane,[1] D. Cronin-Hennessy,[6] R. Culbertson,[5] T. Daniels,[19] F. DeJongh,[7] S. Delchamps,[7] S. Dell'Agnello,[27] M. Dell'Orso,[27] R. Demina,[7] L. Demortier,[31] M. Deninno,[2] P. F. Derwent,[7] T. Devlin,[32] J. R. Dittmann,[6] S. Donati,[27] J. Done,[34] T. Dorigo,[25] A. Dunn,[20] N. Eddy,[20] K. Einsweiler,[18] J. E. Elias,[7] R. Ely,[18] E. Engels, Jr.,[28] D. Errede,[13] S. Errede,[13] Q. Fan,[30] G. Feild,[39] C. Ferretti,[27] I. Fiori,[2] B. Flaugher,[7] G. W. Foster,[7] M. Franklin,[11] M. Frautschi,[35] J. Freeman,[7] J. Friedman,[19] H. Frisch,[5] Y. Fukui,[17] S. Funaki,[36] S. Galeotti,[27] M. Gallinaro,[26] O. Ganel,[35] M. Garcia-Sciveres,[18] A. F. Garfinkel,[29] C. Gay,[11] S. Geer,[7] D. W. Gerdes,[15] P. Giannetti,[27] N. Giokaris,[31] P. Giromini,[9] G. Giusti,[27] L. Gladney,[26] D. Glenzinski,[15] M. Gold,[22] J. Gonzalez,[26]

A. Gordon,[11] A. T. Goshaw,[6] Y. Gotra,[25] K. Goulianos,[31] H. Grassmann,[27] L. Groer,[32] C. Grosso-Pilcher,[5] G. Guillian,[20] R. S. Guo,[33] C. Haber,[18] E. Hafen,[19] S. R. Hahn,[7] R. Hamilton,[11] R. Handler,[38] R. M. Hans,[39] F. Happacher,[9] K. Hara,[36] A. D. Hardman,[29] B. Harral,[26] R. M. Harris,[7] S. A. Hauger,[6] J. Hauser,[4] C. Hawk,[32] E. Hayashi,[36] J. Heinrich,[26] B. Hinrichsen,[14] K. D. Hoffman,[29] M. Hohlmann,[5] C. Holck,[26] R. Hollebeek,[26] L. Holloway,[13] S. Hong,[20] G. Houk,[26] P. Hu,[28] B. T. Huffman,[28] R. Hughes,[23] J. Huston,[21] J. Huth,[11] J. Hylen,[7] H. Ikeda,[36] M. Incagli,[27] J. Incandela,[7] G. Introzzi,[27] J. Iwai,[36] Y. Iwata,[12] H. Jensen,[7] U. Joshi,[7] R. W. Kadel,[18] E. Kajfasz,[25] H. Kambara,[10] T. Kamon,[34] T. Kaneko,[36] K. Karr,[37] H. Kasha,[39] Y. Kato,[24] T. A. Keaffaber,[29] K. Kelley,[19] R. D. Kennedy,[7] R. Kephart,[7] P. Kesten,[18] D. Kestenbaum,[11] H. Keutelian,[7] F. Keyvan,[4] B. Kharadia,[13] B. J. Kim,[30] D. H. Kim,[7a] H. S. Kim,[14] S. B. Kim,[20] S. H. Kim,[36] Y. K. Kim,[18] L. Kirsch,[3] P. Koehn,[23] K. Kondo,[36] J. Konigsberg,[8] S. Kopp,[5] K. Kordas,[14] A. Korytov,[8] W. Koska,[7] E. Kovacs,[7a] W. Kowald,[6] M. Krasberg,[20] J. Kroll,[7] M. Kruse,[30] T. Kuwabara,[36] S. E. Kuhlmann,[1] E. Kuns,[32] A. T. Laasanen,[29] S. Lami,[27] S. Lammel,[7] J. I. Lamoureux,[3] M. Lancaster,[18] T. LeCompte,[1] S. Leone,[27] J. D. Lewis,[7] P. Limon,[7] M. Lindgren,[4] T. M. Liss,[13] J. B. Liu,[30] Y. C. Liu,[33] N. Lockyer,[26] O. Long,[26] C. Loomis,[32] M. Loreti,[25] J. Lu,[34] D. Lucchesi,[27] P. Lukens,[7] S. Lusin,[38] J. Lys,[18] K. Maeshima,[7] A. Maghakian,[31] P. Maksimovic,[19] M. Mangano,[27] J. Mansour,[21] M. Mariotti,[25] J. P. Marriner,[7] A. Martin,[39] J. A. J. Matthews,[22] R. Mattingly,[19] P. McIntyre,[34] P. Melese,[31] A. Menzione,[27] E. Meschi,[27] S. Metzler,[26] C. Miao,[20] T. Miao,[7] G. Michail,[11] R. Miller,[21] H. Minato,[36] S. Miscetti,[9] M. Mishina,[17] H. Mitsushio,[36] T. Miyamoto,[36] S. Miyashita,[36] N. Moggi,[27] Y. Morita,[17] A. Mukherjee,[7] T. Muller,[16] P. Murat,[27] H. Nakada,[36] I. Nakano,[36] C. Nelson,[7] D. Neuberger,[16] C. Newman-Holmes,[7] C-Y. P. Ngan,[19] M. Ninomiya,[36] L. Nodulman,[1] S. H. Oh,[6] K. E. Ohl,[39] T. Ohmoto,[12] T. Ohsugi,[12] R. Oishi,[36] M. Okabe,[36] T. Okusawa,[24] R. Oliveira,[26] J. Olsen,[38] C. Pagliarone,[27] R. Paoletti,[27] V. Papadimitriou,[35] S. P. Pappas,[39] N. Parashar,[27] S. Park,[7] A. Parri,[9] J. Patrick,[7] G. Pauletta,[27] M. Paulini,[18] A. Perazzo,[27] L. Pescara,[25] M. D. Peters,[18] T. J. Phillips,[6] G. Piacentino,[27] M. Pillai,[30] K. T. Pitts,[7] R. Plunkett,[7] L. Pondrom,[38] J. Proudfoot,[1] F. Ptohos,[11] G. Punzi,[27] K. Ragan,[14] D. Reher,[18] A. Ribon,[25] F. Rimondi,[2] L. Ristori,[27] W. J. Robertson,[6] T. Rodrigo,[27] S. Rolli,[37] J. Romano,[5] L. Rosenson,[19] R. Roser,[13] T. Saab,[14] W. K. Sakumoto,[30] D. Saltzberg,[5] A. Sansoni,[9] L. Santi,[27] H. Sato,[36] P. Schlabach,[7] E. E. Schmidt,[7] M. P. Schmidt,[39]

A. Scribano,[27] S. Segler,[7] S. Seidel,[22] Y. Seiya,[36] G. Sganos,[14] M. D. Shapiro,[18] N. M. Shaw,[29] Q. Shen,[29] P. F. Shepard,[28] M. Shimojima,[36] M. Shochet,[5] J. Siegrist,[18] A. Sill,[35] P. Sinervo,[14] P. Singh,[28] J. Skarha,[15] K. Sliwa,[37] F. D. Snider,[15] T. Song,[20] J. Spalding,[7] T. Speer,[10] P. Sphicas,[19] F. Spinella,[27] M. Spiropulu,[11] L. Spiegel,[7] L. Stanco,[25] J. Steele,[38] A. Stefanini,[27] K. Strahl,[14] J. Strait,[7] R. Ströhmer,[7a] D. Stuart,[7] G. Sullivan,[5] K. Sumorok,[19] J. Suzuki,[36] T. Takada,[36] T. Takahashi,[24] T. Takano,[36] K. Takikawa,[36] N. Tamura,[12] B. Tannenbaum,[22] F. Tartarelli,[27] W. Taylor,[14] P. K. Teng,[33] Y. Teramoto,[24] S. Tether,[19] D. Theriot,[7] T. L. Thomas,[22] R. Thun,[20] R. Thurman-Keup,[1] M. Timko,[37] P. Tipton,[30] A. Titov,[31] S. Tkaczyk,[7] D. Toback,[5] K. Tollefson,[30] A. Tollestrup,[7] H. Toyoda,[24] W. Trischuk,[14] J. F. de Troconiz,[11] S. Truitt,[20] J. Tseng,[19] N. Turini,[27] T. Uchida,[36] N. Uemura,[36] F. Ukegawa,[26] G. Unal,[26] J. Valls,[7a] S. C. van den Brink,[28] S. Vejcik, III,[20] G. Velev,[27] R. Vidal,[7] R. Vilar,[7a] M. Vondracek,[13] D. Vucinic,[19] R. G. Wagner,[1] R. L. Wagner,[7] J. Wahl,[5] N. B. Wallace,[27] A. M. Walsh,[32] C. Wang,[6] C. H. Wang,[33] J. Wang,[5] M. J. Wang,[33] Q. F. Wang,[31] A. Warburton,[14] T. Watts,[32] R. Webb,[34] C. Wei,[6] H. Wenzel,[16] W. C. Wester, III,[7] A. B. Wicklund,[1] E. Wicklund,[7] R. Wilkinson,[26] H. H. Williams,[26] P. Wilson,[5] B. L. Winer,[23] D. Winn,[20] D. Wolinski,[20] J. Wolinski,[21] S. Worm,[22] X. Wu,[10] J. Wyss,[25] A. Yagil,[7] W. Yao,[18] K. Yasuoka,[36] Y. Ye,[14] G. P. Yeh,[7] P. Yeh,[33] M. Yin,[6] J. Yoh,[7] C. Yosef,[21] T. Yoshida,[24] D. Yovanovitch,[7] I. Yu,[7] L. Yu,[22] J. C. Yun,[7] A. Zanetti,[27] F. Zetti,[27] L. Zhang,[38] W. Zhang,[26] and S. Zucchelli[2]

(CDF Collaboration)

[1] *Argonne National Laboratory, Argonne, Illinois 60439*

[2] *Istituto Nazionale di Fisica Nucleare, University of Bologna, I-40127 Bologna, Italy*

[3] *Brandeis University, Waltham, Massachusetts 02264*

[4] *University of California at Los Angeles, Los Angeles, California 90024*

[5] *University of Chicago, Chicago, Illinois 60638*

[6] *Duke University, Durham, North Carolina 28708*

[7] *Fermi National Accelerator Laboratory, Batavia, Illinois 60510*

[8] *University of Florida, Gainesville, FL 33611*

[9] *Laboratori Nazionali di Frascati, Istituto Nazionale di Fisica Nucleare, I-00044 Frascati, Italy*

[10] *University of Geneva, CH-1211 Geneva 4, Switzerland*

[11] *Harvard University, Cambridge, Massachusetts 02138*

[12] *Hiroshima University, Higashi-Hiroshima 724, Japan*

[13] *University of Illinois, Urbana, Illinois 61801*

[14] *Institute of Particle Physics, McGill University, Montreal H3A 2T8, and University of Toronto, Toronto M5S 1A7, Canada*

[15] *The Johns Hopkins University, Baltimore, Maryland 21218*

[16] *Universotaet Karlsruhe, 76128 Karlsruhe, Germany*

[17] *National Laboratory for High Energy Physics (KEK), Tsukuba, Ibaraki 315, Japan*

[18] *Ernest Orlando Lawrence Berkeley National Laboratory, Berkeley, California 94720*

[19] *Massachusetts Institute of Technology, Cambridge, Massachusetts 02139*

[20] *University of Michigan, Ann Arbor, Michigan 48109*

[21] *Michigan State University, East Lansing, Michigan 48824*

[22] *University of New Mexico, Albuquerque, New Mexico 87132*

[23] *The Ohio State University, Columbus, OH 43320*

[24] *Osaka City University, Osaka 588, Japan*

[25] *Universita di Padova, Istituto Nazionale di Fisica Nucleare, Sezione di Padova, I-36132 Padova, Italy*

[26] *University of Pennsylvania, Philadelphia, Pennsylvania 19104*

[27] *Istituto Nazionale di Fisica Nucleare, University and Scuola Normale Superiore of Pisa, I-56100 Pisa, Italy*

[28] *University of Pittsburgh, Pittsburgh, Pennsylvania 15270*

[29] *Purdue University, West Lafayette, Indiana 47907*

[30] *University of Rochester, Rochester, New York 14628*

[31] *Rockefeller University, New York, New York 10021*

[32] *Rutgers University, Piscataway, New Jersey 08854*

[33] *Academia Sinica, Taipei, Taiwan 11530, Republic of China*

[34] *Texas A&M University, College Station, Texas 77843*

[35] *Texas Tech University, Lubbock, Texas 79409*

[36] *University of Tsukuba, Tsukuba, Ibaraki 315, Japan*

[37] *Tufts University, Medford, Massachusetts 02155*

[38] *University of Wisconsin, Madison, Wisconsin 53806*

[39] *Yale University, New Haven, Connecticut 06511*

(CDF Collaboration)

Abstract

We describe the properties of six-jet events, with six-jet mass exceeding 520 GeV/c^2, produced at the Fermilab proton-antiproton collider operating at a center-of-mass energy of 1.8 TeV. Observed distributions for a set of 20 multijet variables are compared with predictions from the HERWIG QCD parton shower Monte Carlo program, the NJETS leading order QCD matrix element Monte Carlo program, and a phase-space model in which six-jet events are distributed uniformly over the kinematically allowed region of the six-body phase space. In general the QCD predictions provide a good description of the observed six-jet distributions.

PACS numbers: 12.38Qk, 13.85.-t, 13.85.Hd, 13.87.-a

1 Introduction

The CDF collaboration has recently reported the characteristics of two-jet, three-jet, four-jet, and five-jet events [1] produced at the Tevatron proton-antiproton collider operating at a center-of-mass energy of 1.8 TeV. Results from an analysis of two-jet events with two-jet mass $m_{2J} > 550$ GeV/c^2, three-jet events with $m_{3J} > 600$ GeV/c^2, four-jet events with $m_{4J} > 650$ GeV/c^2, and five-jet events with $m_{5J} > 750$ GeV/c^2 were compared with predictions from (i) the NJETS [2] tree level leading order (TLLO) perturbative Quantum Chromodynamics (pQCD) $2 \rightarrow N$ calculations, (ii) the HERWIG [3] QCD parton shower Monte Carlo program, and (iii) a model in which events are distributed uniformly over the available multijet phase space. In general, both the NJETS and HERWIG calculations were found to provide a good description of the observed multijet distributions for a complete set of $(4N-4)$ multijet variables [4] that span the multibody parameter space in the N-jet rest-frame. More recently, improvements to the NJETS program have enabled us to explore the systematic uncertainties on the QCD predictions and extend our multijet studies to the six-jet topology.

In the present paper the characteristics of six-jet events with six-jet mass $m_{6J} > 520$ GeV/c^2 are compared with predictions from the NJETS matrix element calculation, the HERWIG parton shower Monte Carlo program, and the phase space model calculation. This comparison of the properties of six-jet events with pQCD predictions provides an interesting test of the approximations used in the HERWIG and NJETS QCD calculations, and facilitates a search for new phenomena associated with the production of many hard partons in the final state.

2 Experimental Details

A description of the CDF detector can be found in Ref. [5]. In the following we give a summary of the main details of the CDF detector, jet reconstruction, and event selection requirements that are relevant to results presented in this paper. We use the CDF co-ordinate system in which the origin is at the center of the detector, the z-axis is along the proton beam direction, θ is the polar angle with respect to the z-axis, and ϕ is the azimuthal angle measured around the beam direction.

The six-jet analysis described in the following sections exploits the CDF calorimeters, which cover the pseudorapidity region $|\eta| < 4.2$, where $\eta \equiv -\ln(\tan\theta/2)$. The calorimeters are constructed in a projective tower geometry in (η, ϕ)-space, and are segmented in depth into electromagnetic and hadronic compartments. The calorimeter towers are 0.1 units wide in η. The tower widths in ϕ are 15^o in the central region and 5^o at larger $|\eta|$ (approximately $|\eta| > 1.2$). Jets are reconstructed using an algorithm that forms clusters from localized energy depositions in the calorimeter towers. Calorimeter towers are associated with a jet if their separation from the jet axis in (η, ϕ)-space $\Delta R \equiv (\Delta\eta^2 + \Delta\phi^2)^{1/2} < R_0$. For the analysis described in this paper the clustering cone radius $R_0 = 0.7$ was chosen. With this R_0 a plot of the separation between all jets observed in the data sample described below reveals that, to a good approximation, clusters with separations $\Delta R < 0.8$ are always merged by the jet algorithm into a single jet, and clusters with separations $\Delta R > 1.0$ are never merged. Thus, the effective minimum observable separation between jet axes $\Delta R_{MIN} = 0.9 \pm 0.1$. For each reconstructed jet a four-vector is calculated as follows. The electromagnetic and hadronic compartments of each tower associated with the jet are assigned tower vectors with magnitudes equal to the energy deposited in the tower and with the direction defined by a unit vector pointing from the event vertex to the center of the calorimeter tower (calculated at a depth which corresponds to shower maximum). The jet momentum vector $\vec{p}$ is computed as the vector sum of the tower vectors, and the jet energy E is computed as the scalar sum of the tower energies. Other quantities can then be derived from the jet four-vector, for example, the single-jet mass $m_j \equiv \sqrt{E^2 - p^2}$.

Jet energies are corrected for calorimeter non-linearities, energy deposited in uninstrumented regions and outside of the clustering cone, and energy gained from the underlying event. The jet corrections typically increase jet energies by 25% for jets with transverse energy $E_T \equiv E \sin\theta > 60$ GeV, where θ is the angle between the jet direction and the beam direction. The jet corrections are larger for lower E_T jets, and typically [6] increase jet energies by about 30% (40%) for jets with $E_T = 40$ GeV (20 GeV). After correction, energies of high-E_T jets are measured with a precision σ_E/E of approximately 0.1 and multijet masses calculated from the jet four-vectors are measured with a precision σ_m/m of approximately 0.1. The systematic uncertainty on the jet energy scale is 5% for jets in the central region ($|\eta| < 1.2$). There is an additional systematic uncertainty of 2% on the energy scale of jets at larger $|\eta|$ relative to the corresponding scale for central jets. Further details of the CDF jet algorithm, jet corrections, and jet resolution functions can be found in Ref. [6].

The data, which correspond to an integrated luminosity of 110 pb^{-1}, were recorded using a trigger which required $\sum E_T > 175$ GeV, where the sum is over the transverse energies (E_T) of all calorimeter clusters reconstructed with a simple cluster algorithm in which clusters are initiated by a seed tower with $E_T > 3$ GeV, and consist of the seed tower plus all contiguous towers with

$E_T > 1$ GeV. The cluster transverse energies were calculated assuming an event vertex at the center of the detector ($x = y = z = 0$). In the subsequent analysis, to reject backgrounds from cosmic ray interactions, beam halo, and detector malfunctions, the events were required to have (i) total energy less than 2000 GeV, (ii) a primary vertex reconstructed with $|z| < 60$ cm, (iii) not more than 8 GeV deposited in the hadron calorimeters out-of-time with the proton-antiproton collision, and (iv) missing-E_T significance [7] $S \equiv \not{E}_T$ $/(\sum E_T\ )^{1/2} < 6$ GeV$^{1/2}$, where $\not{E}_T \equiv |\sum \vec{E_T}_i|$, and $\vec{E_T}_i$ is a vector in the transverse plane that points from the interaction vertex to calorimeter cell i and has magnitude equal to the cell E_T. To select events with six or more jets, we require at least six well separated jets ($\Delta R > 0.9$) reconstructed with the CDF jet algorithm with corrected $E_T > 20$ GeV, and jet pseudorapidity $|\eta| < 3$. Finally, we restrict our analysis to the region where the trigger was fully efficient by requiring $\sum E_T > 320$ GeV, where the sum is over the six highest E_T jet transverse energies and the reconstructed vertex position has been used to calculate E_T. These requirements select 5262 events with six or more jets for further analysis.

3 QCD and Phase-Space Predictions

In the following we will compare observed multijet distributions with predictions from (a) the HERWIG [3] QCD parton shower Monte Carlo program, (b) the NJETS [2] TLLO QCD $2 \rightarrow N$ matrix element Monte Carlo program, and

(c) a model in which events are distributed uniformly over the available N-body phase-space.

3.1 The HERWIG Monte Carlo Calculation

HERWIG is a QCD parton shower Monte Carlo program that includes both initial- and final-state gluon radiation. HERWIG predictions can be thought of as QCD $2 \rightarrow 2$ predictions with gluon radiation, color coherence, hadronization, and an underlying event. We have used version 5.6 of the HERWIG Monte Carlo program together with a full simulation of the CDF detector response. In our HERWIG calculations we have used the CTEQ2L [8] parton distribution functions and the scale $Q^2 = stu/2(s^2 + u^2 + t^2)$, where s, t, and u are the Mandelstam variables. The sensitivity of the predictions to the choice of parton distribution function and scale will be discussed in section 6. HERWIG generates $2 \rightarrow 2$ processes above a specified p_T^{hard}, where p_T^{hard} is the transverse momentum of the outgoing partons from the hard scatter before any radiation has occurred. It is important to choose a low value of p_T^{hard} so that adequate account is taken of events in which the detector response has fluctuated upwards by several standard deviations and/or the spectator system accompanying the hard scattering process, including the initial state radiation, makes an unusually large contribution to the measured $\sum E_T$. We have set the minimum p_T^{hard} to 40 GeV/c. The contribution to the $\sum E_T > 320$ GeV Monte Carlo sample from events with $p_T^{hard} < 40$ GeV/c is negligible.

3.2 The NJETS QCD Matrix Element Calculation

NJETS is a $2 \to N$ QCD Monte Carlo program based on the exact TLLO QCD matrix element for $N < 6$. However, for $N = 6$, NJETS uses an approximation to the TLLO $2 \to 6$ matrix element in which (i) the non-leading-order-in-color contributions are neglected [9], and (ii) all non-zero helicity amplitudes contributing to the $2 \to 6$ matrix element are assumed to be equal. More specifically, only a subset of the helicity amplitudes are computed, namely those for which all but two of the partons have the same helicity. This approximation, which is referred to as the special helicity (SPHEL) approximation, is described more fully in Ref. [10], where it has been shown to give reasonable predictions of event shapes for $N = 2$, 3, 4, and 5, although the absolute multijet cross sections tend to be poorly estimated. The leading color and SPHEL approximations simplify the calculations and greatly speed up the numerical evaluation of the matrix element, enabling statistically precise predictions to be made with available computing resources.

Using the NJETS Monte Carlo program together with the CTEQ3L parton distribution parametrizations [8] and the renormalization scale $Q^2 = < P_T^2 >$, we have generated approximately 1 million six-jet events that pass the $\sum E_T$, jet E_T, and jet separation cuts described in section 2. NJETS is a parton level generator, and does not include a hadronization model or interface to the CDF detector simulation. Therefore, to simulate the experimental jet energy resolution we have applied a Gaussian energy smearing to the parton energies with $\sigma_{E_T} = 0.1 \times E_T$, which provides a good approximation to the measured jet resolution function for jets with $E_T > 100$ GeV. Lower E_T jets are measured with a degraded resolution, for example, $\sigma_{E_T} = 0.15 \times E_T$ for jets with $E_T = 30$ GeV. In section 6 we show that degrading the assumed resolution function within this range does not significantly change the NJETS predictions described in this paper.

3.3 Phase-Space Model

We have used the GENBOD program [11] to generate samples of Monte Carlo events for which the six-jet systems uniformly populate the 6-body phase-space. These phase-space Monte Carlo events were generated with six-jet masses distributed according to the corresponding observed m_{6J} distribution. The masses of the individual jets (m_j) were generated to reproduce the observed single-jet mass-fraction (f_j) distribution, where $f_j \equiv m_j/m_{6J}$. Comparisons between the resulting phase-space model distributions and the corresponding HERWIG and NJETS Monte Carlo distributions help us to understand which multijet parameters are most sensitive to the behaviour of the QCD six-jet matrix element.

4 Six-Jet Variables

To completely describe a six-jet system in the six-jet rest frame we need 21 independent parameters. However, we can rotate the six-jet system about the beam axis without losing any interesting physical information. Hence in practice we only require 20 variables. We will use the twenty variables introduced and described in Ref. [4] to study the six-jet kinematics. Consider the process $1 + 2 \to 3 + 4 + 5 + 6 + 7 + 8$ where the incoming partons are labeled 1 and 2, and the six outgoing jets are labeled 3, 4, 5, 6, 7, and 8. The outgoing jets are ordered according to their energies in the six-jet rest frame:

$$E_3 > E_4 > E_5 > E_6 > E_7 > E_8 \, . \tag{1}$$

The first variable we choose is the six-jet mass, m_{6J}. To define the remaining 19 variables we begin by reducing the six-body system to a three-body system by merging jets. This requires 3 steps:

$$\begin{aligned} 3+4+5+6+7+8 &\longrightarrow 3' + 4' + 5' + 6' + 7' && (2) \\ &\longrightarrow 3'' + 4'' + 5'' + 6'' && (3) \\ &\longrightarrow 3''' + 4''' + 5''' \, . && (4) \end{aligned}$$

In each step we merge the two objects with the lowest two-body mass. The two jets merged in the first step are labelled E and F, where $E_E > E_F$, and E_E and E_F are the energies of E and F in the six-jet rest-frame. The two objects merged in the second step are labelled C' and D', where $E_{C'} > E_{D'}$, and the primes remind us that C' and D' are defined after one merging step has already taken place. The two objects merged in the third step are labelled A'' and B'', where $E_{A''} > E_{B''}$, and the double primes remind us that A'' and B'' are defined after two merging steps have already been performed.

We are now ready to define the six-jet variables. To do this we start by defining 7 variables that completely specify the $(3''', 4''', 5''')$-system, and then define a further 12 variables that describe the three steps in which two bodies were merged. To completely specify the three-body ($3'''$, $4'''$, $5'''$)-system in the three-body rest-frame we must specify the masses of the three bodies, and four additional parameters that specify the position of the three-body system in the three-body parameter space. We begin by ordering the three bodies such that $E_{3'''} > E_{4'''} > E_{5'''}$, where the $E_{j'''}$ are energies in the three-body rest-frame. In analogy with the standard analysis of three-jet systems we can then define four dimensionless variables, $X_{3'''}$, $X_{4'''}$, $\cos\theta_{3'''}$, and $\psi_{3'''}$:

(i) The Dalitz variables $X_{3'''}$ and $X_{4'''}$, where:

$$X_{j'''} \equiv \frac{2E_{j'''}}{m_{6J}}. \tag{5}$$

(ii) The cosine of the leading-body scattering angle:

$$\cos\theta_{3'''} \equiv \frac{\vec{P}_{AV} \cdot \vec{P}_{3'''}}{|\,\vec{P}_{AV}\,||\,\vec{P}_{3'''}\,|}, \tag{6}$$

where $\vec{P}_{AV}$ is the average beam direction in the six-jet (= three-body) rest-frame:

$$\vec{P}_{AV} \equiv \vec{P}_1 - \vec{P}_2, \tag{7}$$

and particle 1 is the incoming parton with the highest energy in the laboratory frame.

(iii) $\psi_{3'''}$, defined as the angle between the three-body plane and the plane containing the highest energy body and the average beam direction:

$$\cos\psi_{3'''} \equiv \frac{(\vec{P}_{3'''} \times \vec{P}_{AV}) \cdot (\vec{P}_{4'''} \times \vec{P}_{5'''})}{|\,\vec{P}_{3'''} \times \vec{P}_{AV}\,||\,\vec{P}_{4'''} \times \vec{P}_{5'''}\,|}. \tag{8}$$

Finally, to specify the masses of the three-bodies we use the three single-body mass fractions $f_{3'''}$, $f_{4'''}$, and $f_{5'''}$, where:

$$f_{j'''} \equiv \frac{m_{j'''}}{m_{6J}}. \tag{9}$$

To complete the specification of a six-jet event we must now specify the three steps in which two bodies were merged. Each step requires four parameters to describe how the composite object has been built from two four-vectors. Hence we must specify twelve parameters in total. Consider a step in which objects i and j (with $E_i > E_j$) get merged:

$$\vec{P}_{ij} = \vec{P}_i + \vec{P}_j \,. \tag{10}$$

Given $\vec{P}_{ij}$, we must now specify $\vec{P}_i$ and $\vec{P}_j$. We need four variables which we define:

(a) The normalized masses f_i and f_j, where

$$f_i \equiv \frac{m_i}{m_{6J}} \quad \text{and} \quad f_j \equiv \frac{m_j}{m_{6J}}. \tag{11}$$

(b) The energy-sharing variable X_i defined in the six-jet rest frame:

$$X_i \equiv \frac{E_i}{E_i + E_j}. \tag{12}$$

(c) The angular variable ψ_{ij} defined as the angle between the plane containing the (ij)-system and the average beam direction, and the plane spanned by objects i and j. The cosine of this angle can be written as:

$$\cos\psi_{ij} \equiv \frac{(\vec{P}_i \times \vec{P}_j)\cdot(\vec{P}_{ij} \times \vec{P}_{AV})}{|\,\vec{P}_i \times \vec{P}_j\,||\,\vec{P}_{ij} \times \vec{P}_{AV}\,|}. \tag{13}$$

In summary, the 20 independent variables that span the six-jet parameter space in the six-body rest-frame are m_{6J}, $X_{3'''}$, $X_{4'''}$, $\cos\theta_{3'''}$, $\psi_{3'''}$, $f_{3'''}$, $f_{4'''}$, $f_{5'''}$, $f_{A''}$, $f_{B''}$, $X_{A''}$, $\psi_{A''B''}$, $f_{C'}$, $f_{D'}$, $X_{C'}$, $\psi_{C'D'}$, f_E, f_F, X_E, and ψ_{EF}.

5 Results

In the following we will compare the observed single-differential distributions with HERWIG, NJETS, and phase space model predictions for the 20 variables defined in the previous section. The definition of six-jet events is inclusive. If there are more than six jets in an event, the six jets with the highest transverse energies are used to define the six-jet system. Since we required $\sum E_T > 320$ GeV, jet $E_T > 20$ GeV, jet $\mid \eta \mid < 3$, and $\Delta R > 0.9$, some regions of the 20-dimensional parameter space are excluded. To reduce the effect of these regions of zero acceptance on the shapes of the one-dimensional distributions we are studying, we apply three additional cuts to the six-jet sample: $m_{6J} > 520$ GeV/c^2, $\mid \cos\theta_{3'''} \mid < 0.9$, and $X_{3'''} < 0.9$. After these requirements we have 1282 events with six or more jets for further analysis, of which 168 events have seven jets, and 26 events have more than seven jets. Examples of four typical six-jet events are shown in Fig. 1.

5.1 Six-Jet-Mass and Three-Body-Dalitz Distributions

The observed six-jet mass distribution (Fig. 2) extends to masses above 1 TeV/c^2, and is well described by both the HERWIG QCD parton shower Monte Carlo and the NJETS predictions. In Fig. 3 the observed three-body Dalitz distribution ($X_{3'''}$ vs $X_{4'''}$) is compared with HERWIG, NJETS, and phase space model predictions. The phase-space population is not uniform over the kinematically allowed region of the $(X_{3'''}, X_{4'''})$-plane, but tends to be depleted at large values of $X_{3'''}$ and $X_{4'''}$. Both the observed and the QCD predicted Dalitz distributions exhibit an excess over the phase-space model predictions as $X_{4'''}$ becomes large, i.e. when the three-body system approaches a two-body topology (note that the energy fraction taken by the third-to-highest-energy body $X_{5'''} \to 0$ as $X_{4'''} \to 1$). Figure 4 shows the projections on the $X_{3'''}$ and $X_{4'''}$ axes. Both the HERWIG and NJETS distributions are similar to the observed $X_{3'''}$ and $X_{4'''}$ distributions. In particular, both QCD calculations can account for the factor of four increase in event density with respect to the phase-space model that is observed at the largest $X_{4'''}$.

5.2 Three-Body Angular Distributions

The observed event population in the $(\cos\theta_{3'''}, \psi_{3'''})$-plane is compared with HERWIG, NJETS, and phase-space model predictions in Fig. 5. Both the observed and the QCD Monte Carlo event populations exhibit enhanced densities in the regions where $| \cos\theta_{3'''} | \to 1$ and $\psi_{3'''} \to 0$ or π. This feature has also been observed in the corresponding three-jet, four-jet, and five-jet event distributions [1], and reflects the shape of the leading order QCD $2 \to 2$ scattering angular distribution, and the preference of the QCD matrix element for planar topologies ($\psi_{3'''} \to 0$ or π). Note that the phase-space model Monte Carlo events are distributed more uniformly over the $(\cos\theta_{3'''}, \psi_{3'''})$-plane, although the analysis cuts imposed on the data sample do produce some regions of reduced experimental acceptance, for example at small $| \cos\theta_{3'''} |$. The regions of reduced acceptance are consequences of the minimum jet-jet separation requirement, and the minimum jet transverse energy requirement. Further discussion can be found in Ref. [4]. Figure 6 displays the $\cos\theta_{3'''}$ and $\psi_{3'''}$ distributions. The observed distributions are very different from the phase-space model predictions. Both the NJETS matrix element calculation and the HERWIG parton shower Monte Carlo calculation give reasonable descriptions of the observed $\cos\theta_{3'''}$ and $\psi_{3'''}$ distributions, although there is some indication that the HERWIG predictions tend to underestimate the rate of events with planar topologies ($\psi_{3'''} \to 0$ or π). Note that the $\cos\theta_{3'''}$ distribution is also similar to the leading order $2 \to 2$ scattering distribution.

5.3 Single-Body Masses for the Three-Body System

The distributions of the normalized single-body masses, which are shown in Fig. 7, exhibit broad peaks at large $f_{j'''}$ that correspond to objects j''' composed of two or more jets, and narrower peaks at low $f_{j'''}$, which correspond to objects j''' that are single jets. Both the NJETS and the HERWIG Monte Carlo programs correctly describe the high-mass parts of the $f_{j'''}$ distributions, which peak at lower values than predicted by the phase-space model, reflecting the preference of the QCD matrix element for soft and collinear final state radiation. The HERWIG QCD Monte Carlo calculation also gives a reasonable description of the observed low-mass region of the $f_{j'''}$ distributions. However, it should be noted that there is a tendency, observed in previous multijet analyses [1], for HERWIG to predict slightly lower single-jet masses than observed. Note that the HERWIG fragmentation model has not been tuned to CDF data. Since NJETS is a parton-level calculation it does not predict the single-jet-mass part of the $f_{j'''}$ distributions.

5.4 Two-Body Energy-Sharing and Angular Distributions

The observed X_j distributions are shown in Fig. 8. Both QCD predictions favor a more asymmetric energy sharing than the phase-space model, reflecting the soft gluon radiation pole in the QCD matrix element. The HERWIG QCD parton shower Monte Carlo program gives a good description of the energy sharing between the two-body sub-systems. The NJETS predictions overestimate the event rate in the large X_j region, i.e. the region that corresponds to a very asymmetric energy sharing. This failure of the NJETS predictions, which is most noticeable for the X_E distribution, is expected as we approach the region of phase space for which there are large corrections to the TLLO predictions associated with soft gluon radiation. The HERWIG parton shower Monte Carlo performs the soft gluon resummations within the framework of the leading log algorithm, and consequently might be expected to give a better description of the energy sharing distributions in the soft gluon radiation region.

The two-body angular distributions are shown in Fig. 9. The observed $\psi_{A''B''}$, $\psi_{C'D'}$, and ψ_{EF} distributions are not very different from the phase-space model predictions, although both the HERWIG and NJETS predictions are seen to give a better description of the data.

5.5 Single-Body Masses for Two-Body Systems

The observed $f_{A''}$, $f_{B''}$, $f_{C'}$, $f_{D'}$, f_E, and f_F distributions are shown in Fig. 10. The single-jet mass peaks in the low-mass parts of these distributions are reasonably well described by the HERWIG predictions, although once again there is a tendency for the predictions to slightly overestimate the rate of low-mass jets. Since NJETS is a parton-level calculation it makes no prediction for the single-jet mass part of the single-body mass distributions. The $f_{A''}$, $f_{B''}$, $f_{C'}$, and $f_{D'}$ distributions also exhibit a long tail at higher masses, reflecting the contributions from multijet systems. Both the HERWIG and NJETS calculations successfully describe these high-mass tails.

6 χ^2/dof Test and Systematic Studies

We have seen that both of the QCD Monte Carlo calculations give a reasonable description of the 20 observed distributions presented in this paper, although there are some differences for specific distributions. To gain a more quantitative understanding of the level of agreement, in Table 1 we list the χ^2/dof (χ^2 per degree of freedom) that characterize the agreement between observations and predictions for each distribution, where:

$$\chi^2/dof \equiv \frac{\sum_{i=1}^{N_{bins}} \frac{(n_i - p_i)^2}{(\sigma_{ni}^2 + \sigma_{pi}^2)}}{N_{bins} - 1}, \tag{14}$$

and n_i and p_i are the number of events in bin i of the observed and predicted distributions respectively, and σ_{ni} and σ_{pi} are the corresponding statistical uncertainties. We have restricted the χ^2 tests for the single-body mass fraction variables to the regions $f_{3'''} > 0.1$, $f_{4'''} > 0.1$, $f_{5''} > 0.1$, $f_{A''} > 0.07$, and $f_{B''} > 0.07$. The low mass parts of these distributions have been excluded because (i) NJETS provides no prediction for the single-jet mass part of the single-body mass fraction distributions, and (ii) the HERWIG Monte Carlo program plus CDF detector simulation provides only a poor description of the single-jet mass distributions. To examine the quality of the overall description of the observed distributions provided by the QCD predictions we exclude the single-body mass fraction variables and confine ourselves to the 11 other distributions ($m_{6J}, X_{3''}, X_{4''}$, $\cos\theta_{3'''}, \psi_{3'''}$, $X_{A''}$, $\psi_{A''B''}, X_{C'}$, $\psi_{C'D'}, X_E$, and ψ_{EF}). We find that the overall χ^2 is 138 for 110 dof for the HERWIG parton shower Monte Carlo predictions, and 146 for 110 dof for the NJETS TLLO QCD matrix element predictions.

The χ^2's discussed so far have not taken into account the systematic uncertainty on the QCD predictions associated with the choice of renormalization scale, parton distribution function, the assumed minimum separation between jets, or for NJETS the assumed jet energy resolution function. Therefore, we have used the NJETS program to predict the distributions for 16 variables (excluding f_E, f_F, $f_{C'}$, and $f_{D'}$) using the renormalization scale choices $\mathrm{Q}^2 = m_{6J}^2$ and $\mathrm{Q}^2 = < p_T^2 >$ (where p_T refers to the transverse momenta of the outgoing partons), the parton distribution choices MRSG [12], GRV94 [13], and CTEQ3L, the minimum jet separation set to $\Delta R = 0.8$, 0.9, and 1.0, and the assumed jet energy resolution degraded to $\sigma_{E_T} = 0.15 E_T$. The χ^2/dof characterizing the agreement between these NJETS calculations and the observed distributions are summarized in Table 2. Note, for example, that choosing the scale $Q^2 = m_{6J}^2$ we obtain an overall χ^2 of 123 for 110 dof. Hence we conclude that, within the systematic uncertainties, the QCD calculations are able to provide an excellent overall description of the six-jet distributions studied in this paper. However, it should be noted that the χ^2/dof for the NJETS X_E distribution is poor for all the parameter choices.

Finally, we have made a number of systematic studies to ensure that our observed six-jet distributions are not significantly distorted due to contributions from multiple interactions, or significantly changed when the jet energy scale is changed by one standard deviation. In particular, to check that additional jets from multiple interactions do not significantly distort our results, we have repeated the six-jet analysis using a low instantaneous luminosity sub-sample ($\mathcal{L} < 7 \times 10^{30}$ cm^{-2} s^{-1}) and a high instantaneous luminosity sub-sample ($\mathcal{L} > 7 \times 10^{30}$ cm^{-2} s^{-1}). To ensure that the uncertainty on the jet energy scale does not give rise to a large uncertainty on the observed multijet distributions we have also repeated the analysis varying the jet energy scale by $\pm 5\%$. In no case do we see significant changes in the observed six-jet distributions. In Table 3 we summarize the NJETS and HERWIG χ^2/dof for each distribution after restricting the analysis to the high or low instantaneous luminosity subsamples, or changing the energy scale. The overall χ^2/dof that describe the agreement between the QCD predictions and the high instantaneous-luminosity (low instantaneous-luminosity) sub-samples for the 11 variables listed above are 1.2 (1.1) for the HERWIG predictions, and 1.3 (1.1) for the NJETS predictions. Hence, although we observe no obvious distortion in the observed distributions at higher luminosities, there is some evidence from the χ^2 test that the agreement between the data and QCD predictions improves at lower luminosities where the contributions from multiple interactions are small. Note that the overall agreement between the observed distributions and both the NJETS and HERWIG QCD predictions is excellent for the low luminosity sub-sample. The overall χ^2/dof that describe the agreement between the QCD predictions and the $+5\%$ (-5%) energy scale distributions for the 11 variables listed above are 1.5 (1.1) for the HERWIG predictions, and 1.4 (1.3) for the NJETS predictions. Hence within the uncertainties on the energy scale we can obtain excellent overall agreement between the QCD predictions and the observed distributions.

7 Conclusions

We have compared the 20 observed six-jet distributions corresponding to the variables introduced in Ref. [4] with HERWIG QCD parton shower Monte Carlo predictions, NJETS QCD Monte Carlo predictions, and phase-space Monte Carlo predictions. We find that:

(i) Many of the observed distributions are sensitive to the underlying QCD matrix element; i.e. the distributions are reasonably well described by the QCD predictions but are significantly different from the phase-space model predictions. This is true for the $X_{4'''}$, $\cos\theta_{3'''}$, $\psi_{3'''}$, $f_{3'''}$, $f_{4'''}$, $f_{5'''}$, $f_{A''}$, $f_{B''}$, $X_{A''}$, and $X_{C'}$ distributions.

(ii) The HERWIG QCD parton shower Monte Carlo calculation gives a good description of all the observed distributions, except perhaps (a) the $\psi_{3'''}$ distribution for which the observed events tend to be more planar than the Monte Carlo predicts, and (b) the single-jet peaks in the single-body mass fraction distributions where the HERWIG fragmentation model plus CDF detector simulation seems to slightly underestimate the single-jet masses. Similar trends have been noted in our previous three-jet, four-jet, and five-jet studies [1].

(iii) The NJETS QCD Monte Carlo calculation gives a good description of the observed distributions except perhaps for the energy sharing distributions X_j, for which the TLLO QCD matrix element calculation tends to overestimate the event rate as the soft gluon radiation pole is approached.

Note that, since NJETS is a parton-level calculation it does not predict the single-jet peaks in the single-body mass fraction distributions. This limits the comparison between the NJETS predictions and the observed distributions for some of the multijet variables.

Finally, we can compare the observed six-jet distributions with the corresponding distributions observed in our previous three-jet, four-jet, and five-jet studies [1]. The multijet variables we are using facilitate this comparison [4]. There are striking similarities between the six-jet distributions and the corresponding multijet distributions observed for three-jet, four-jet, and five-jet events. In particular we note that:

(a) The distributions of the three-body variables ($X_{3'''}$, $X_{4'''}$, $\cos\theta_{3'''}$, and $\psi_{3'''}$) are very similar to the corresponding four-jet and five-jet distributions reported in Ref. [1]. For example, all of the $\cos\theta_3$ distributions are well described by the LO $2 \to 2$ scattering form, and all of the X_4 distributions show an excess over the phase-space model prediction of about a factor of 4 at $X_4 = 0.875$.

(b) The $f_{3'''}$, $f_{4'''}$, and $f_{5'''}$ distributions exhibit multibody peaks at similar positions to the corresponding peaks observed in the earlier four-jet and five-jet analyses, namely at values of $f_3 \sim 0.2$, $f_4 \sim 0.15$, and $f_5 \sim 0.12$.

(c) The distributions that describe the two-body systems ($f_{A''}$, $f_{B''}$, $X_{A''}$, $\psi_{A''B''}$, $f_{C'}$, $f_{D'}$, $X_{C'}$, $\psi_{C'D'}$, f_E, f_F, X_E, and ψ_{EF}) are qualitatively similar to the corresponding four-jet and five-jet distributions reported in Ref. [1]. Of these distributions, the two-body energy sharing distributions and, for the six-jet events, the $f_{A''}$, and $f_{B''}$ distributions, are very different from the phase-space model predictions.

We conclude that both the NJETS and HERWIG QCD predictions provide a reasonable description of the kinematics of six-jet production at high multijet mass. There are striking similarities between the observed three-jet, four-jet, and five-jet multijet distributions presented in our previous publication, and the six-jet multijet distributions presented in this paper which, together with the ability of the parton shower Monte Carlo to describe the detailed characteristics of the multijet events, suggests that $2 \to 2$ scattering plus initial and final-state gluon radiation provides a good approximation to the kinematics predicted by the complete QCD matrix element.

Acknowledgements

We thank the Fermilab Accelerator Division and the technical and support staff of our respective institutions. This work was supported by the U.S. Department of Energy, the U.S. National Science Foundation, the Istituto Nazionale di Fisica Nucleare of Italy, the Ministry of Science, Culture and Education of Japan, the Natural Sciences and Engineering Research Council of Canada, the National Science Council of the Republic of China, and the A.P. Sloan Foundation.

References

[1] F. Abe *et al.* (CDF Collaboration), Phys. Rev. **D54**, 4221 (1996).

[2] F. A. Berends, W. Giele, and H. Kuijf, Nucl. Phys. **B333**, 120 (1990).

[3] G. Marchesini *et al.*, Comp. Phys. Commun. **67** (1997) 465.

[4] S. Geer and T. Asakawa, Phys. Rev. **D53**, 4793 (1996).

[5] F. Abe *et al.* (CDF Collaboration), Nucl. Instrum. and Methods, **A271**, 387 (1988).

[6] F. Abe *et al.* (CDF Collaboration), Phys. Rev. **D45**, 1448 (1992).

[7] F. Abe *et al.* (CDF Collaboration), Phys. Rev. **D45**, 2249 (1992).

[8] H.L. Lai *et al.*, Phys. Rev. **D51**, 4763 (1995)

[9] F. Berends and H. Kuijf, Phys. Lett. **232B**, 266 (1989).

[10] F. Berends and H. Kuijf, Nucl. Phys. **B353**, 59 (1991).

[11] CERN Program Library Manual 1989.10.03, Routine W515, p. 6.503.

[12] A.D. Martin, R.G. Roberts, and W.J. Stirling, Phys. Rev. **D50**, 6734 (1994).

[13] M. Gluck, E. Reya, and R. Vogt, Z. Phys. **C67**, 433 (1995).

Table 1: The χ^2/dof characterizing the level of agreement between HERWIG, NJETS, and phase-space model predictions and the observed distributions for 16 of the 20 variables discussed in the text. The χ^2/dof are not given for the $f_{C'}$, $f_{D'}$, f_E, and f_F distributions which are dominated by the single-jet mass distribution and therefore not predicted by the NJETS calculation, and poorly described by the HERWIG calculation. The numbers in parentheses correspond to the remaining single-body mass distributions which, although not dominated by the single-jet mass peak, nevertheless do exhibit a single-jet mass peak and are therefore not used in computing the overall χ^2/dof in the bottom line of the table.

		χ^2/dof		
Parameter	# of dof	HERWIG	NJETS	Phase Space
m_{6j}	13	1.0	1.9	—
$X_{3'''}$	8	1.5	2.2	1.3
$X_{4'''}$	7	1.3	0.6	7.7
$\cos\theta_{3'''}$	18	1.0	0.5	62.2
$\psi_{3'''}$	10	2.9	0.6	40.
$f_{3'''}$	(10)	(1.0)	(1.5)	(43.)
$f_{4'''}$	(8)	(1.4)	(1.9)	(38.)
$f_{5'''}$	(8)	(2.2)	(4.1)	(8.8)
$f_{A''}$	(7)	(0.7)	(3.1)	(24.)
$f_{B''}$	(7)	(1.4)	(5.5)	(12.)
$X_{A''}$	8	1.5	1.5	17.1
$\psi_{A''B''}$	10	1.2	0.3	5.9
$X_{C'}$	8	2.2	2.2	27.
$\psi_{C'D'}$	10	1.6	0.7	1.0
X_E	8	0.8	5.4	1.4
ψ_{EF}	10	0.9	2.0	2.3
Overall	110	1.3	1.3	17.0

Table 2: The χ^2/dof characterizing the level of agreement between NJETS predictions and the observed distributions for 16 of the 20 variables discussed in the text, tabulated for alternative choices of the renormalization scale, minimum jet separation, parton distribution function, and the assumed jet energy resolution function degraded so that $\sigma_{E_T} = 0.15E_T$. The numbers in parentheses correspond to the single-body mass distributions which, although not dominated by the single-jet mass peak, nevertheless do exhibit a single-jet mass peak and are therefore not used in computing the overall χ^2/dof in the bottom line of the table.

Parameter	# of dof	χ^2/dof					
		$Q^2 = M^2$	$\Delta R = 0.8$	$\Delta R = 1.0$	MRSG	GRV94	$\sigma_{E_T} = 0.15E_T$
m_{6j}	13	0.7	1.3	1.6	0.7	0.7	1.6
$X_{3'''}$	8	1.1	1.2	1.1	1.6	1.7	1.4
$X_{4'''}$	7	0.9	0.4	0.3	0.4	0.4	0.8
$\cos\theta_{3'''}$	18	1.4	1.5	0.6	1.1	0.9	0.9
$\psi_{3'''}$	10	0.7	1.2	1.8	1.1	1.0	1.7
$f_{3'''}$	(10)	(1.5)	(2.8)	(0.7)	(1.5)	(1.4)	(1.7)
$f_{4'''}$	(8)	(2.9)	(3.6)	(1.8)	(2.6)	(2.7)	(4.3)
$f_{5'''}$	(8)	(3.2)	(4.3)	(3.0)	(3.3)	(3.2)	1.7)
$f_{A''}$	(7)	(2.9)	(5.1)	(3.3)	(3.6)	(3.2)	(4.3)
$f_{B''}$	(7)	(6.1)	(9.4)	(3.1)	(5.2)	(6.2)	(7.5)
$X_{A''}$	8	1.1	2.3	1.2	1.4	1.5	1.2
$\psi_{A''B''}$	10	1.2	1.1	0.9	1.0	0.8	1.0
$X_{C'}$	8	1.6	2.5	1.7	1.6	1.7	3.5
$\psi_{C'D'}$	10	0.7	0.8	0.5	0.7	0.5	0.9
X_E	8	3.5	7.8	5.0	6.0	6.2	3.8
ψ_{EF}	10	1.1	1.8	2.0	1.6	1.3	1.0
Overall	110	1.1	1.7	1.3	1.3	1.2	1.4

Table 3: The χ^2/dof characterizing the level of agreement between NJETS (HERWIG) predictions and the observed distributions for 16 of the 20 variables discussed in the text, tabulated for high luminosity ($> 7\times10^{30}$ cm^{-2}s^{-1}) and low luminosity ($< 7\times10^{30}$ cm^{-2}s^{-1}) subsamples, and for the overall data sample analyzed with the jet energy scale increased and decreased by 5%. The overall χ^2/dof in the bottom line of the table are for the 11 non-single-body mass variables.

Parameter	χ^2/dof			
	High Lum.	Low Lum.	105% E-Scale	95% E-Scale
	NJETS (HERWIG)	NJETS (HERWIG)	NJETS (HERWIG)	NJETS (HERWIG)
m_{6j}	2.2 (1.1)	1.3 (1.0)	0.7 (1.7)	2.0 (0.6)
$X_{3'''}$	1.4 (0.9)	2.4 (2.0)	2.9 (1.5)	1.6 (0.8)
$X_{4'''}$	0.8 (1.0)	0.2 (1.1)	0.8 (1.6)	0.5 (0.9)
$\cos\theta_{3'''}$	0.7 (1.3)	0.3 (0.6)	0.6 (1.6)	0.7 (1.0)
$\psi_{3'''}$	0.7 (1.6)	0.5 (2.8)	0.8 (4.0)	1.0 (2.8)
$f_{3'''}$	0.5 (1.3)	2.2 (0.8)	2.4 (0.9)	0.9 (1.1)
$f_{4'''}$	1.9 (1.8)	1.3 (0.9)	2.4 (1.4)	0.9 (0.8)
$f_{5'''}$	2.4 (2.2)	2.2 (2.0)	5.9 (1.8)	2.8 (2.1)
$f_{A''}$	1.8 (0.8)	1.7 (0.4)	5.3 (1.1)	2.1 (1.3)
$f_{B''}$	2.3 (0.6)	3.8 (1.2)	7.4 (1.8)	4.6 (1.7)
$X_{A''}$	2.6 (2.5)	0.6 (0.7)	1.3 (1.0)	1.5 (1.3)
$\psi_{A''B''}$	0.8 (1.7)	0.5 (0.7)	0.6 (1.1)	0.4 (0.9)
$X_{C'}$	1.0 (1.1)	2.0 (1.7)	2.7 (2.5)	2.7 (1.8)
$\psi_{C'D'}$	0.6 (0.5)	0.8 (2.0)	0.9 (1.8)	0.6 (2.0)
X_E	4.1 (1.2)	4.0 (0.6)	6.1 (0.7)	4.1 (1.0)
ψ_{EF}	1.6 (1.2)	1.6 (0.5)	2.7 (0.8)	1.6 (0.7)
Overall	1.3 (1.2)	1.1 (1.1)	1.4 (1.5)	1.3 (1.1)

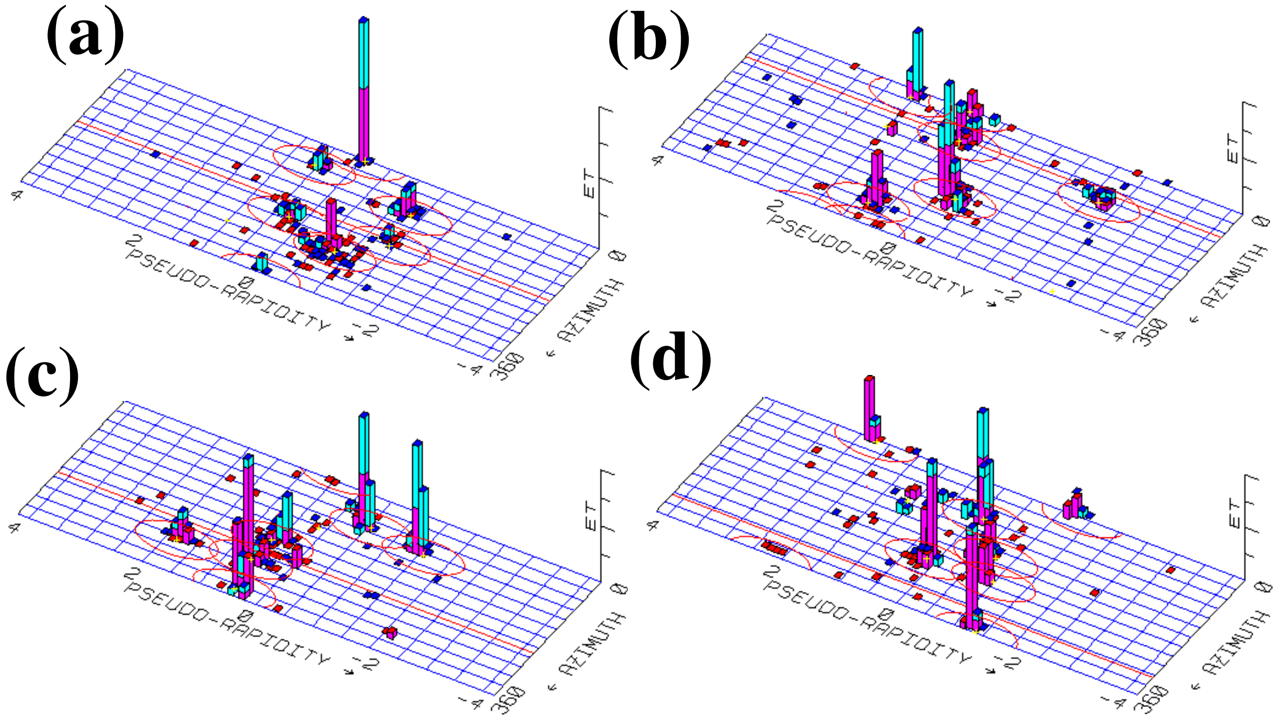

Figure 1: Four typical six-jet events. The transverse energy flow measured in the CDF calorimeters is shown in the (η, ϕ)-plane for an event with (a) $m_{6J} = 679$ GeV/c^2, $X_{3'''} = 0.72$, $X_{4'''} = 0.70$, $\cos\theta_{3'''} = -0.55$, $\psi_{3'''} = 2.4$, (b) $m_{6J} = 691$ GeV/c^2, $X_{3'''} = 0.81$, $X_{4'''} = 0.75$, $\cos\theta_{3'''} = 0.82$, $\psi_{3'''} = 2.3$, (c) $m_{6J} = 772$ GeV/c^2, $X_{3'''} = 0.88$, $X_{4'''} = 0.60$, $\cos\theta_{3'''} = -0.84$, $\psi_{3'''} = 1.1$, (d) $m_{6J} = 672$ GeV/c^2, $X_{3'''} = 0.72$, $X_{4'''} = 0.66$, $\cos\theta_{3'''} = 0.80$, $\psi_{3'''} = 2.9$.

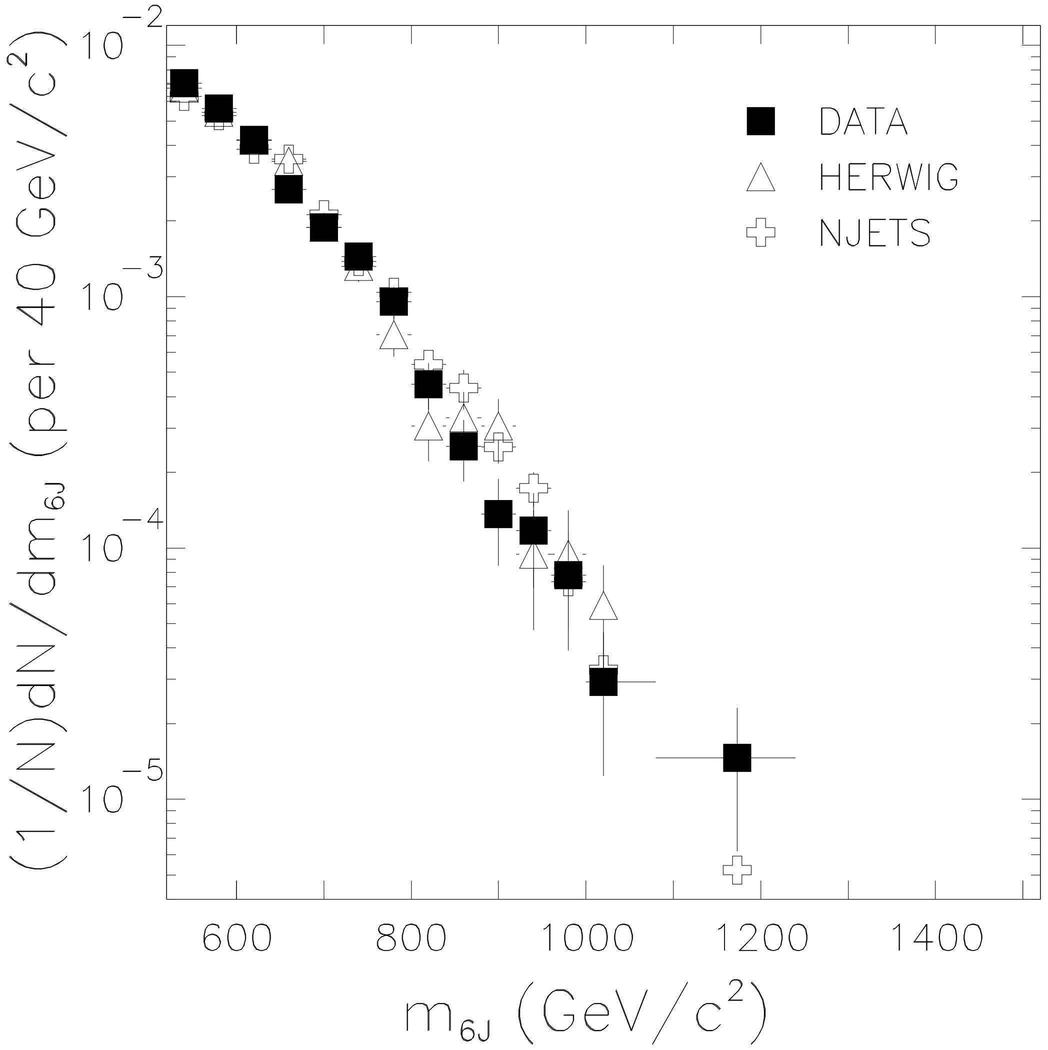

Figure 2: The six-jet mass spectra for data, HERWIG QCD predictions, and NJETS QCD predictions after requiring $m_{6J} > 520$ GeV/c^2, $|\cos\theta_{3'''}| < 0.9$, and $X_{3'''} < 0.9$.

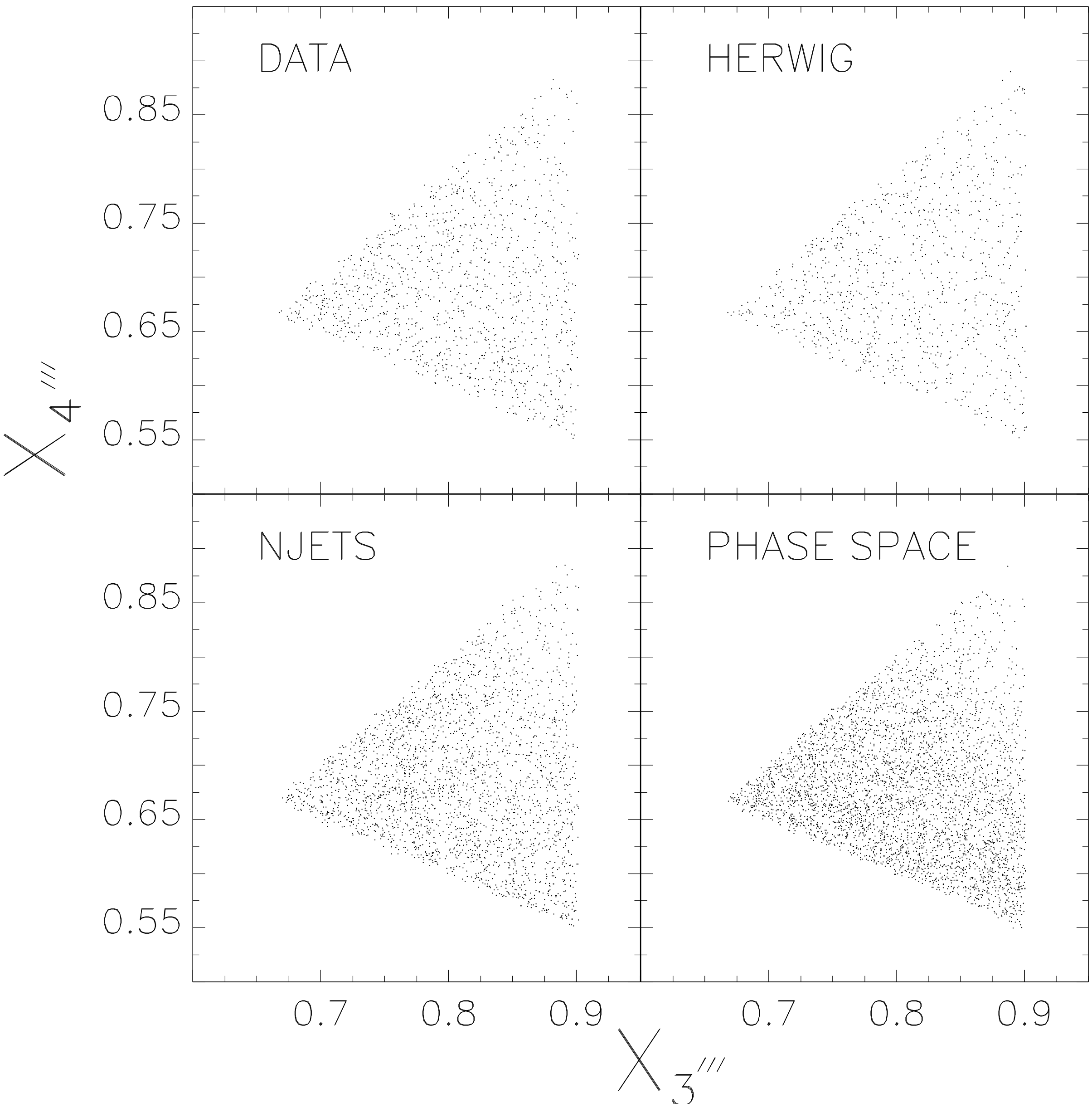

Figure 3: Inclusive three-body Dalitz plots after requiring $m_{6J} > 520$ GeV/c^2, $|\cos\theta_{3'''}| < 0.9$, and $X_{3'''} < 0.9$.

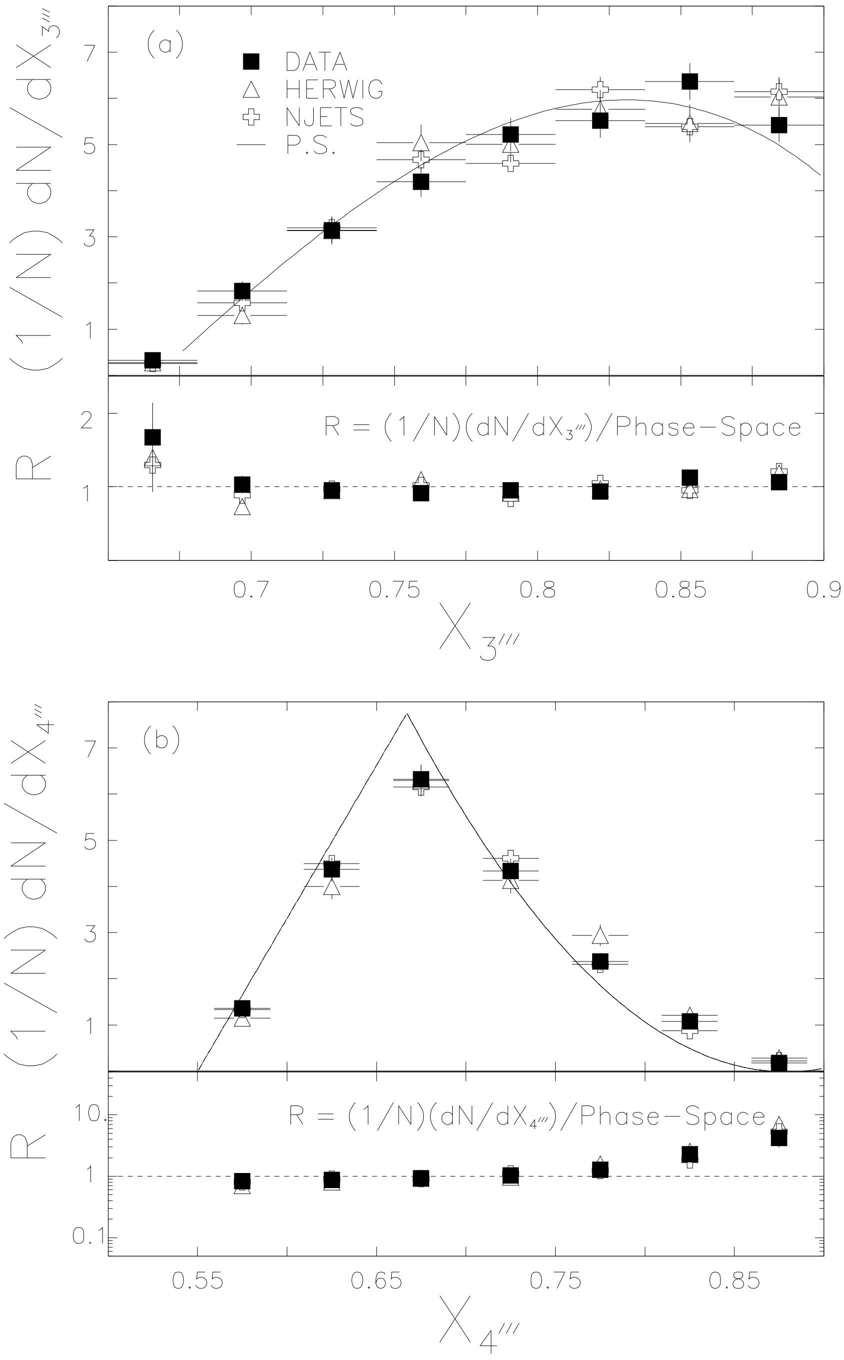

Figure 4: Dalitz distributions for events that satisfy the requirements $m_{6J} > 520$ GeV/c^2, $|\cos\theta_{3'''}| < 0.9$, and $X_{3'''} < 0.9$.

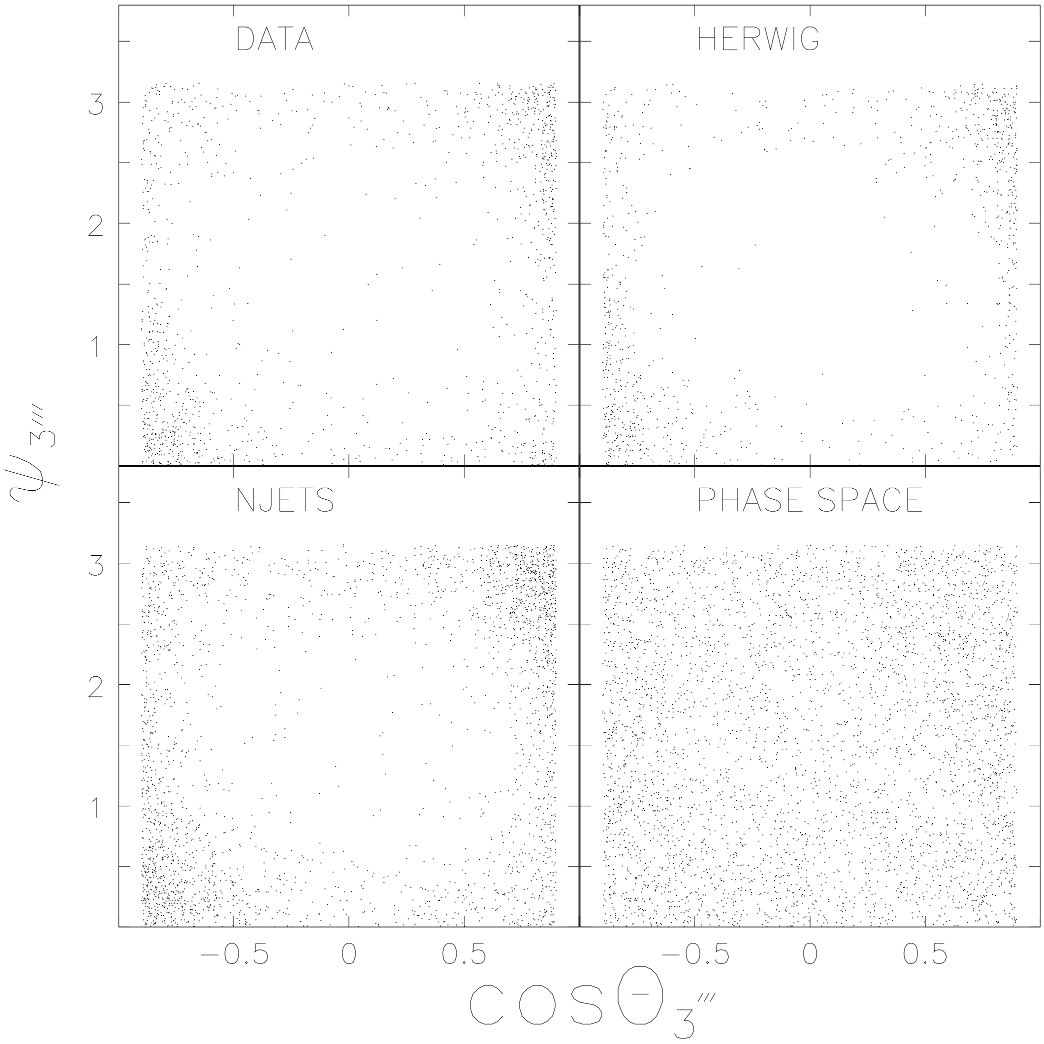

Figure 5: Event populations in the $(\cos\theta_{3'''}, \psi_{3'''})$-plane, shown for events that satisfy the requirements $m_{6J} > 520$ GeV/c^2, $|\cos\theta_{3'''}| < 0.9$, and $X_{3'''} < 0.9$..

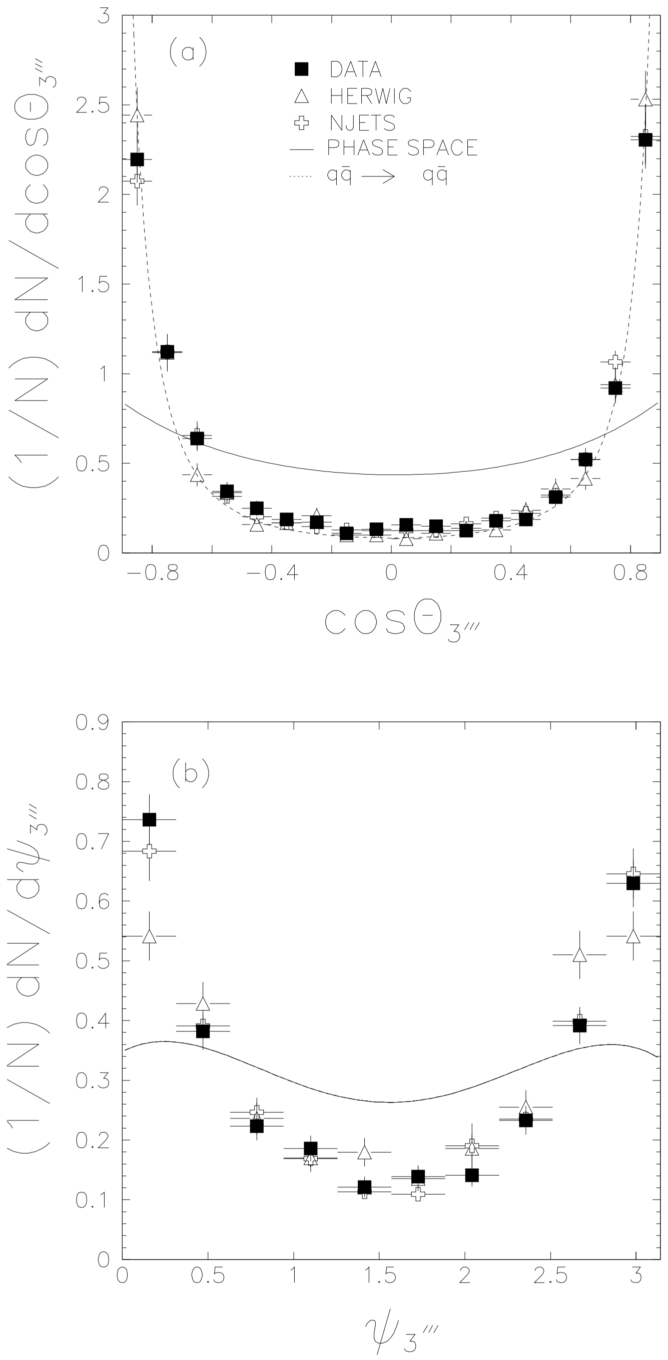

Figure 6: $\cos\theta_{3'''}$ and $\psi_{3'''}$ distributions after applying the following cuts: $m_{6J} > 520$ GeV/c^2, $\mid \cos\theta_{3'''} \mid < 0.9$, and $X_{3'''} < 0.9$. The measured distributions are compared with HERWIG, NJETS, and phase-space model predictions, and for the $\cos\theta_{3'''}$ distribution, with the leading-order quark-antiquark scattering distribution.

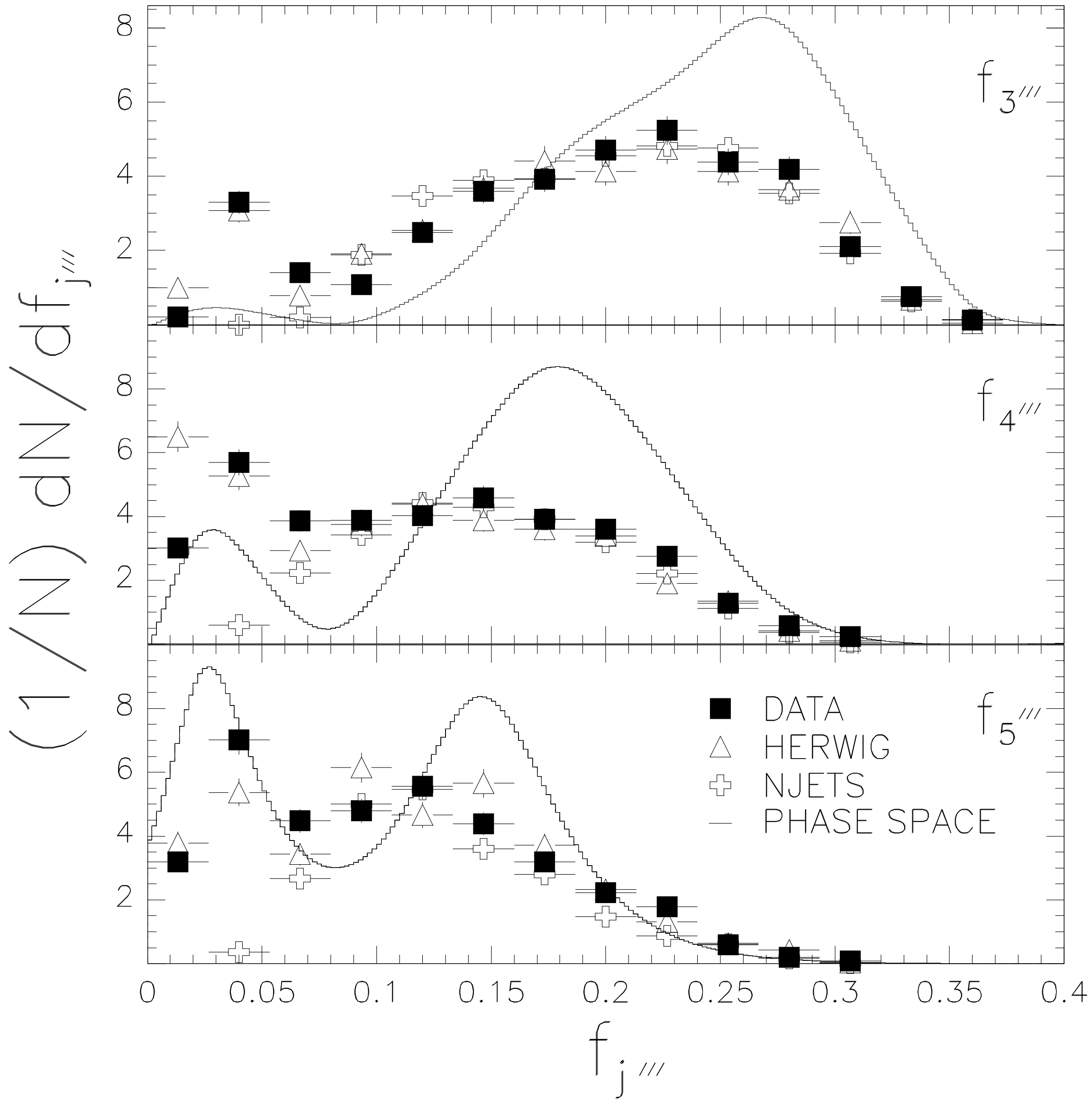

Figure 7: The normalized single-body mass distributions in the three-body system for data (solid squares), the HERWIG QCD predictions (triangles), the NJETS QCD predictions (crosses), and the phase-space predictions (histograms).

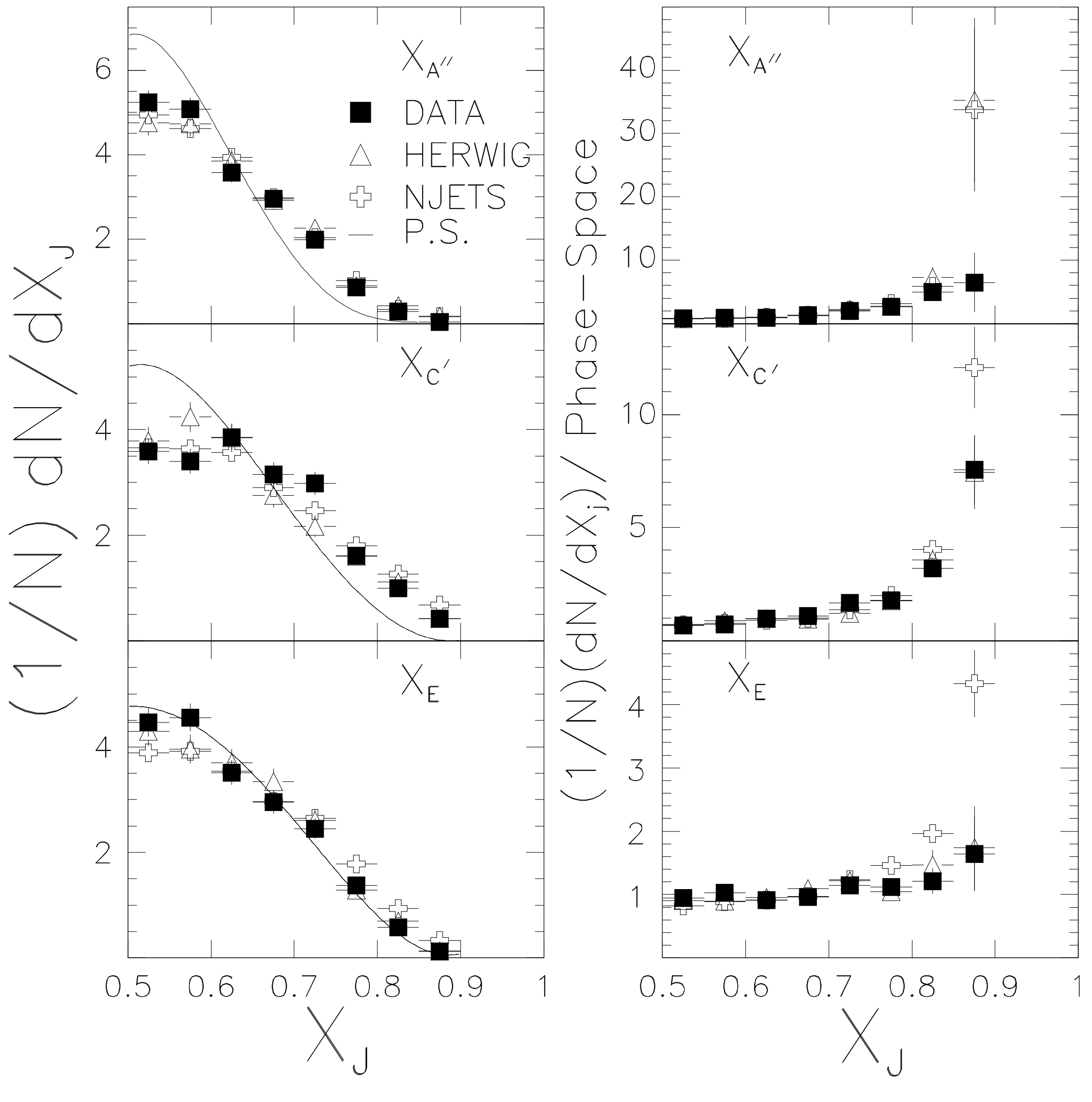

Figure 8: The two-body energy sharing distributions for data (solid squares), the HERWIG QCD predictions (triangles), the NJETS QCD predictions (crosses), and the phase-space predictions (curves).

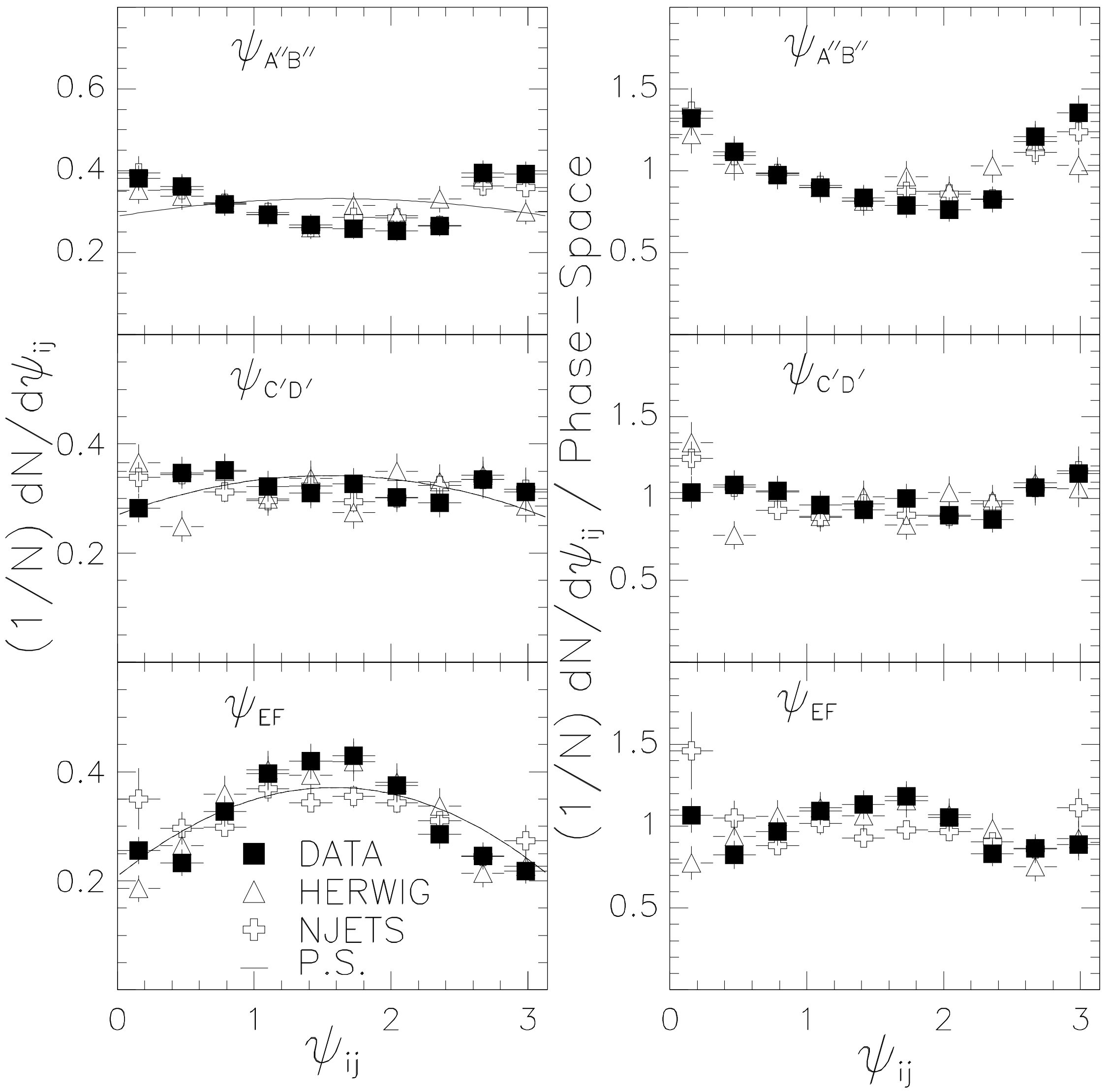

Figure 9: The two-body angular distributions for data (solid squares), the HERWIG QCD predictions (triangles), the NJETS QCD predictions (crosses), and the phase-space predictions (curves).

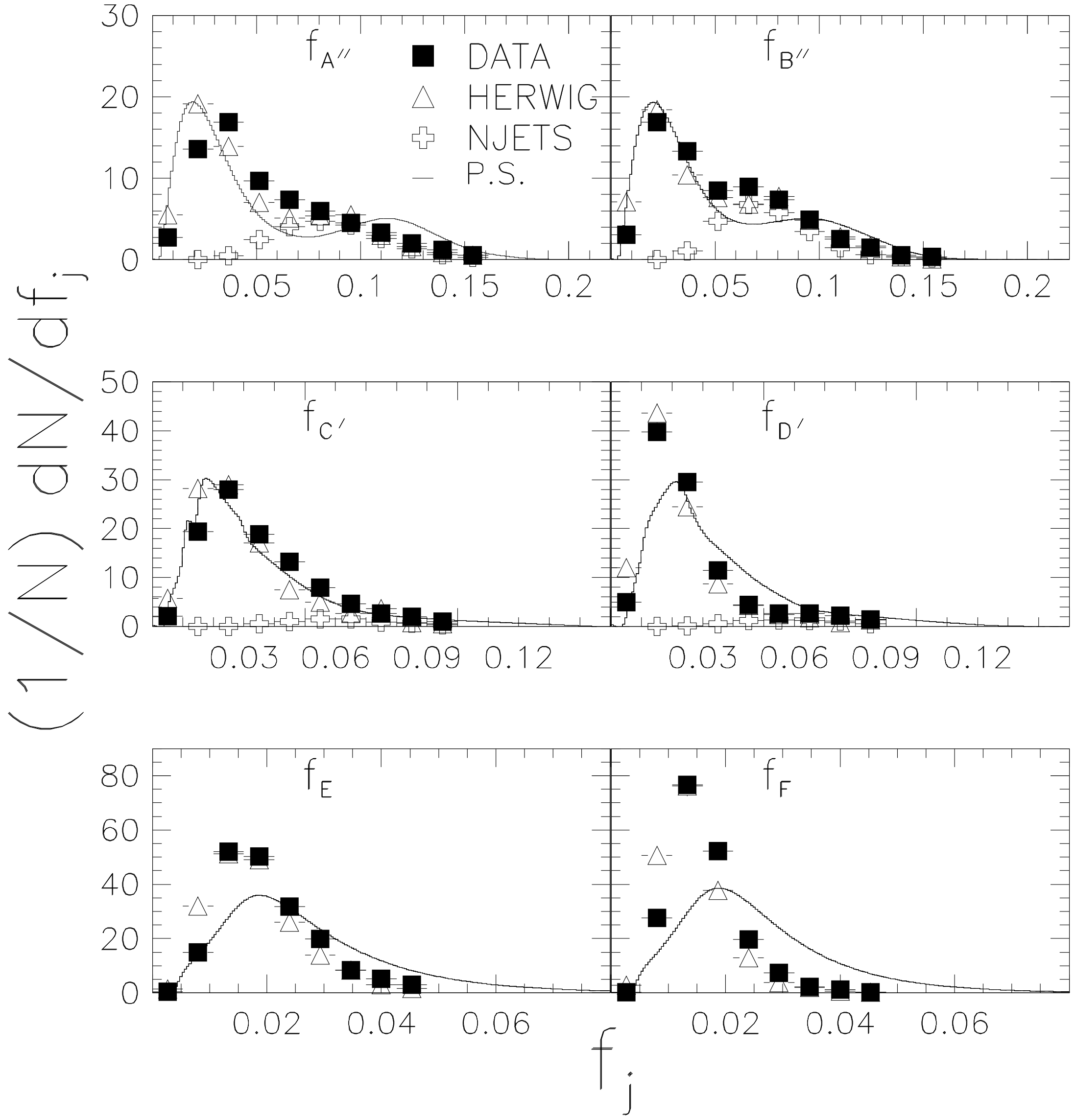

Figure 10: The normalized single-body mass distributions in the two-body systems for data (solid squares), the HERWIG QCD predictions (triangles), the NJETS QCD predictions (crosses), and the phase-space predictions (curves).